



# Computational Investigation of Porous Media Combustion Technology in Spark Ignition Engine

Debojit Sharma<sup>1</sup> · Biplab Kumar Debnath<sup>1</sup>

Received: 18 February 2018 / Accepted: 12 February 2019 / Published online: 4 March 2019  
© Shiraz University 2019

## Abstract

In the present work, computational fluid dynamics approach is adopted to study the possibility of using porous media in combustion and emission in a single-cylinder four-stroke spark ignition engine. The combustion behavior inside the engine without and with application of porous media is studied. The analysis with application of PM signifies enhanced combustion behavior. The compression ratio is kept at 7. Two different types of fluid computational domains are considered, namely, without and with PM. The three-dimensional modeling, meshing and simulations of the combustion chambers are performed with the ANSYS 17.1-FLUENT software. The  $k-\epsilon$  turbulence model, the premixed combustion model and the spark ignition model are used in the study. The parameters to be analyzed are the variation of cylinder pressure, temperature and turbulence at different crank angles. The results of the computational work without PM are validated with the experimental work, which is executed on the research engine setup operated in SI mode. The work is performed at different engine loads by varying the engine torque, viz. 6 Nm (25%), 12 Nm (50%), 18 Nm (75%) and 24 Nm (100%) along with the no-load condition. The analyses of the results indicate that the peak value of total pressure (1,986,868.99 Pa) and average value of total temperature (632.63 K) with PM at 100% load are lower than without PM (1,992,314.50 Pa and 604.81 K). The concentrations of NO<sub>x</sub> emissions are significantly reduced by the use of PM for all the loads. The percentage reductions in NO<sub>x</sub> emissions at no load, 25%, 50%, 75% and 100%, are found to be 2.5%, 11.1%, 9.4%, 9% and 2.12%, respectively.

**Keywords** Porous media · Spark ignition · Combustion · Load · Peclet number

## List of Symbols

### Notations

$b$	Inertial resistance ( $\text{m}^{-1}$ )
$B$	Bore (mm)
$c_p$	Specific heat (J/kg)
$D$	Diameter (mm)
$h$	Clearance height (mm)
$H$	Height of the computational domain (mm)
$\Sigma H$	Heat of combustion (J/kg)
$k$	Thermal conductivity (W/m K)
$K$	Permeability ( $\text{m}^2$ )
$l^{1/2}$	Characteristics length of the effective pore diameter (mm)

$L$	Height of the PM (mm)
$P$	Cylinder pressure (Pa)
$r_c$	Compression ratio
$Q$	Heat release in a process ( $J^\circ$ )
$s$	Laminar flame speed (cm/s)
$S$	Sphericity of the pores
$T$	Adiabatic temperature (K)
$V$	Cylinder volume ( $\text{m}^3$ )

### Greek Symbols

$\alpha, \beta$	Burned gas diluents fraction
$\gamma$	Specific heat capacity ratio
$\delta$	Laminar flame thickness (mm)
$\eta$	Thermal efficiency
$\theta$	Crank angle ( $^\circ$ )
$\mu$	Dynamic fluid viscosity ( $\text{N s/m}^2$ )
$\rho$	Fluid density ( $\text{kg/m}^3$ )
$\Phi$	Mean equivalence ratio
$\nu$	Kinematic viscosity ( $\text{m}^2/\text{s}$ )
$\phi$	Porosity

✉ Biplab Kumar Debnath  
biplab.debnath@nitm.ac.in  
Debojit Sharma  
sharmadebojit3@gmail.com

<sup>1</sup> ME Department, NIT Meghalaya, Shillong,  
Meghalaya 793003, India

## Subscripts

$p$	Pore
$m$	Mean
$u$	Unburnt
$s, g$	Solid and fluid phase

## Abbreviations

ATDC	After top dead center (°)
BTDC	Before top dead center (°)
BDC	Bottom dead center
C	Computational
CAD	Crank angle degree (°)
CI	Compression ignition
E	Experimental
HRR	Heat release rate ( $J^\circ$ )
ICE	Internal combustion engine
PM	Porous media
PPI	Pore per inch

## 1 Introduction

The rapid advancement in the technology and improved living standards of the society is responsible for the rise in the abundant use of the fossil fuels. This poses a couple of harmful indications attributed by fast depletion of the fossil resources, along with the environmental pollution. Researchers all around the world are trying various combinations of technologies to accomplish homogenous mixture formation. One such technique to realize homogenous mixture formation in internal combustion engines (ICE) is porous medium (PM) combustion. The PM combustion is advantageous compared to free flame combustion, since it delivers homogeneous combustion process, higher burning rates, low emissions of the pollutants, to name a few. A porous media (PM) can be defined as the substance having inter-connected voids or pores. The skeletal of the PM is often called the matrix or frame. Many natural materials such as rock and soil obtained from aquifers, petroleum reservoirs, zeolites, biological tissues of bones, woods, cork, man-made materials, such as cements and ceramics can be called as PM (Patel et al. 2015). The specific properties of PM, especially the ceramic ones, which are attributed to the homogeneous combustion are the high specific heat, high melting point, lower thermal expansion coefficient and good thermal and compressive strength, etc. (Das et al. 2015). Permeability is directly proportional to the increase of porosity (Liu et al. 2009). Tensile strength of PM is found to be inversely proportional to the increase of porosity. The longevity of a material under fatigue at high stress level is markedly reduced by a small amount of porosity. This is because the pores turn as sites for the initiation of crack and its growth (Shi et al. 2011). There are different applications

of PM, namely filtration, acoustics, soil mechanics, petroleum engineering, bioremediation, geophysics, etc. (Weclas 2005). Some of the advantages of using PM are:

- Large specific surface area of PM improves the homogeneity of the combustion (Das et al. 2015).
- The addition of PM in a compressor or expander provides the thermal stability during the compression or expansion process. As a result, the thermodynamic efficiency of the system increases for a fixed power density (Weclas 2005).
- High heat capacity of PM controls the combustion temperature over a wide range of mixture compositions (Krishna et al. 2016).
- PM acts as flame stabilizer during combustion process and helps to trim down the harmful gases like  $NO_x$ , CO etc. (Zhao and Lai 1995).

From 1917 onward, numerous researchers patented the application of PM in different areas by varying its geometrical and material properties. Later on, PM was used to improve the individual engine process, especially the intake system and the combustion chamber (Park and Kaviyani 2002). The greater portion of the literature was written during the last 10–15 years, while the awareness of the role and potential of the PM combustion technology on IC engine gradually increased.

The novel concept of the utilization of PM in direct-injection CI engines to achieve a homogeneous combustion of a well-premixed charge was developed by Weclas and Durst in the year 2001. They performed a systematic experimental study on a test engine, which was a modified diesel engine by inserting a silicon carbide (SiC) PM into the cylinder head between the intake and exhaust valves. Fuel was injected into the PM volume, and consequently, all combustion events, i.e., fuel vaporization, fuel air mixture formation and homogenization, as well as combustion reactions, occurred inside the PM. Their results showed the extraordinary characteristics of the PM engine in comparison with the conventional one, such as very low emissions, high cycle efficiency and low combustion noise (Durst and Weclas 2001).

A real three-dimensional (3D) porous structure positioned downstream of the throttle of the engine carburetor was proposed by Schladitz and Hutzenlaub as described in a German patent in 1978. A system with very similar in operation was proposed by Bernecker, 1978, where carburetor has a housing filled with ceramic pieces (as a porous element) fulfilling the task of vaporization and homogenization. A liquid-fuel vaporizer concept was proposed by Gladigow and Schaetzling in a US patent in 1997. In this case, an additional pre-chamber containing a porous structure was localized in the engine head between intake and exhaust valves. Another

system with a porous element for in-cylinder engine application was proposed by Mueller as described in a German patent application in 1975. In 1984, Siewert proposed a catalytic grid to be applied in proximity to the fuel injector of a gasoline direct-injection engine. The concept was suggested for utilizing a late direct gasoline injection strategy for a stratified charge with catalytic ignition (Durst and Weclas 2001). The effects of PM properties on the fuel injection parameters, spray characteristics and multi-jet splitting effects have been investigated experimentally by Navid and Jamil in the year 2010. They found the rich core zone of the spray reduces in the presence of PM. Further, a better interaction between fuel and air is encountered at various fuel injection pressures (Shaahangian and Ghoje 2010). However, in both cases the PM is applied to the locations, which do not have any motion during combustion. Hence, the extent of deposition of carbon on PM and the use of PM for the long-run is not clear from the earlier studies. The thermal regeneration concept for diesel engines is explained by Park and Kaviany (2002) for in-cylinder reciprocating porous regenerator. During the regenerative heating stroke (compression stroke), as the temperature and pressure of the charge inside the cylinder increase, there is subsequent heating of the PM surface. The interaction between the compressed charge and the heated surface of PM results in a rapid chemical reaction between fuel and air. Whereas during the cooling stroke, i.e., expansion stroke, the exhaust charge deposits some sensible heat, which gets stored in the PM. This stored energy is further utilized for heating the fresh charge during the suction stroke. This enhances the reaction rate resulting in improved thermal efficiency (Polasek and Macek 2003). Hanamura et al. (1997) performed one-dimensional numerical study on a reciprocating heat engine with superadiabatic combustion in PM. The results showed that the thermal diffusion by radiation decreases in the PM, and the maximum temperature increases. This results in the extension of the flammability limit for the heat engine. Jugjai and Polmart (2003) developed a novel down-flow compact burner without the need of using a spray atomizer. They introduced a packed bed emitter installed downstream of the porous burner. The results of the experiment revealed an efficient method for enhancement of evaporation and combustion of the liquid fuels without a spray atomizer. As per the physics described by Nield and Bejan (2006), the topology (3D interconnected porosity) of PM triggers the generation of small turbulence scales in the flow motions. This continuously breaks down the thermal boundary layer causing effective heat transfer (Nield and Bejan 2006). As a result, the heat transfer rate between the reactant mixtures is further enhanced by the increased specific surface area and high emissivity. In SI engine, this type of study is yet to be performed. Further, there is hardly any literature, which reports the application of PM in modified

piston in SI engine. To date, the PM is reported to be applied in the cylinder head, valves or in the pre-chamber near to the fuel injector. However, for small-scale diesel engines (viz. 3.5 kW), which are found to be used as pump sets, small gen sets for decentralized locality, etc., there is a clearance volume ranging between 30 and 80 cc. The applications of PM in this small volume range at the aforementioned locations will barely produce any significant improvement of combustion because of the limitation in size. Further, during the occurrence of combustion all these parts remain still. The only dynamic component during combustion is the piston. If PM is fixed in the piston top, then the dynamicity of piston will induce a relative motion between the combustible products inside and outside the PM. This will eliminate any chances of formation of carbon deposits inside PM. Armed with the improved combustion characteristics, this will benefit the SI engine performance in the long run. Further, the 3D topology of the PM will induce localized turbulence scales, which will help with better fuel–air mixing (Zhou et al. 2014). This, coupled with the high heat capacity of the ceramic PM, will provide the regenerative heat transfer for the incoming fresh charge and reduce the fuel consumption. Patel et al. (2015) performed a technical review on the study of effect of PM combustion chamber on diesel engine performance and emission based on PMs like SiC, Al<sub>2</sub>O<sub>3</sub> mixture, Ni Cr Al foam, ZrO<sub>2</sub> foam, which were mounted on the cylinder head. According to them, the efficiency of diesel engine can be increased from 37 to 56% by using PM combustion chamber. Shahangian and Ghojel (2010) performed experimental work to investigate the role of PM in homogenization of high-pressure diesel fuel spray combustion and found the efficiency of combustion to be lower in the PM cases relative to the free jet ones. Mohammadi et al. (2012) performed a computational work on simulation of open PM engine that was carried out with KIVA-3V code, in which methane was injected directly in hot cylindrical PM mounted in the engine head. They found that at early stage of expansion, for almost any injection duration, solid phase of PM prevents the temperature of gas phase and combustion products from increasing. This reduces the NO production drastically (Mohammadi et al. 2012). Zhou et al. (2014) created a numerical model for combustion processes in PM with porous burners with porosity 0.87, 0.8, 0.7, respectively. They found that at all equivalence ratios, lower levels of HC, NO<sub>x</sub> and CO are generated in the PM engine compared with the equivalent engine without PM (Zhou et al. 2014). Liu et al. (2009) performed computational work of a porous medium (PM) engine using a 2-zone combustion model and found that the combustion process in the PM zone is relatively steady and is a function of the initial PM temperature. Jamalabadi et al. (2015) performed computational work on effect of fuel injection angle on the thermal behavior of a 2D axisymmetric non-premixed methane–air flame in vertical

cylinder filled by porous media. It was found that porous combustion reduces the temperature with more uniform distribution throughout the domain (Jamalabadi et al. 2015). Chidambaram and Thulasi (2016) developed a mathematical model for analyzing the combustion, performance and emission characteristics of a conventional engine and a cylinder head PM engine. The developed mathematical model was found to be suitable for the prediction of the combustion and performance characteristics of the conventional and the cylinder head PM engines.  $\text{NO}_x$  emission was found to be relatively lower in the cylinder head PM engine. CO and HC emissions were found to be lower than the conventional engine owing to the complete vaporization and clean combustion of fuel (Chidambaram and Thulasi 2016). There are many theoretical models based on the application of PM proposed by the researchers in the past few years. The majority of previous works reported on PM are limited to the experimentation in a constant volume chamber. Only a limited number of works have been reported on simulation model of PM engines and that too was confined to gaseous fuels. In this work, an attempt is made to predict the performance and emission characteristics of PM engine using liquid fuels (Patel et al. 2015; Shahangian and Ghajel 2010; Mohammadi et al. 2012; Zhou et al. 2014; Liu et al. 2009; Jamalabadi et al. 2015; Chidambaram and Thulasi 2016). The effects of major PM parameters on the SI engine performance, which have not yet been reported in earlier literature, will also be studied in the proposed work.

## 2 Experimental Setup for Baseline Tests

In order to perform the computational work, some SI (spark ignition) engine parameters are needed to be considered as per an experimental setup. The specifications of the same are obtained from an engine in SI mode, available at NIT Meghalaya, and are presented in Table 1.

A four-stroke, single-cylinder, water-cooled, vertical engine coupled to an eddy current dynamometer is

considered for the current study. The engine compression ratio is varied by using a screw rod and a hand wheel assembly, which actuates an auxiliary piston. Depending on the fuel type, the provisions are made for mounting each spark plug and diesel injector (one at a time) at the same hole on the cylinder head. The present work is based on the traditional petrol engine run in SI mode. For petrol run, carburetor and ignition arrangement, are made. Since in the carbureted engine fuel–air mixture is supposed to be in almost stoichiometric condition, the same is considered during the start of simulation. The display panel is equipped with digital indicators for measuring air flow rate, fuel flow rate, torque, temperature, cooling water flow, speed and signal conditioner for  $PV-P\theta$  (interface unit). A load controller is mounted on the same panel for varying different loads to be applied in the engine crank shaft. A cantilever-type load cell is mounted on the loading end of the dynamometer to sense the engine load, which provides the readings in terms of torque (Nm) by digital torque indicator. It is also provided with necessary sensors and transmitters for recording combustion pressure with respect to the various crank angles. All these signals are interfaced to computer through signal conditioner and signal converter for computerized data acquisition. The schematic diagram of experimental setup is presented in Fig. 1.

## 3 Computational Analysis

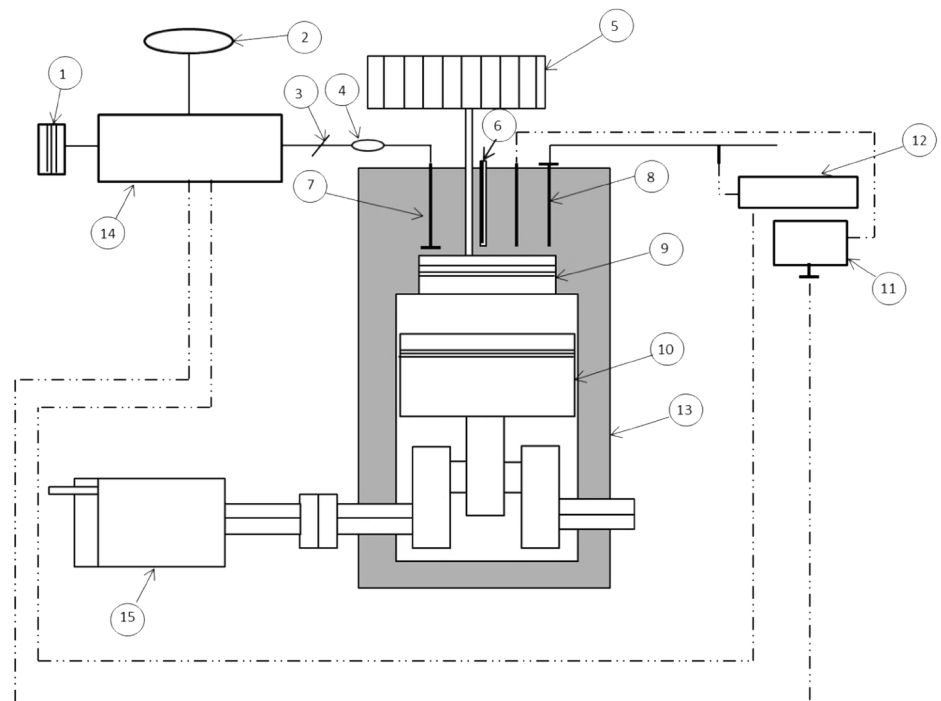
The flow mechanism, heat transfer and the behavior of combustion in PM can be explicitly analyzed with the help of computational fluid dynamics (CFD) (Zhou et al. 2014). The CFD tool ANSYS 17.1-FLUENT is used in the present work. It uses finite volume approach to discretize the governing equations, which are solved using implicit method. The second-order upwind scheme has been used for spatial discretization of the convective terms. The diffusion term is differenced centrally with second order to obtain better accuracy in the results (Fluent 6.3 Documentation 2010).

### 3.1 Computational Modeling

In the present work, CFD approach is adopted to study the possibility of using PM in combustion and emission in a single-cylinder four-stroke SI engine. Two different computational domains are prepared to perform the study, namely without and with PM. The geometrical models of computational domain (without and with PM) are shown in Fig. 2. The porous volume is considered by removing the hemispherical bowl volume of diameter 52 mm and attaching a cylindrical PM in it of the same diameter. The solid volume in the PM should be equal to the solid part removed from the hemispherical bowl so that the same compression ratio is maintained. The height of the PM

**Table 1** Baseline engine specifications

Parameters	Size and features
Make and model	Kirloskar TV1
Type	Single-cylinder, four-stroke petrol, water cooled
Power	5.2 kW (6.97 BHP) at 1500 rpm
Stroke, $L$ (mm)	110
Bore, $B$ (mm)	87.5
Compression ratio, CR	7:1
Capacity (cc)	661
Spark timing ( $^\circ$ BTDC)	48

**Fig. 1** Schematic diagram of the experimental setup

1	Air filter	6	Spark plug	11	Computer
2	Fuel tank	7	Inlet valve	12	Exhaust gas calorimeter
3	Throttle valve	8	Outlet valve	13	Cylinder wall
4	Carburettor	9	Auxiliary piston	14	Display panel
5	Screw rod	10	Engine piston	15	Eddy current dynamometer

should be 26 mm. The spark timing is the standard set by the manufacturer at  $48^\circ$  BTDC. Hence, the height of the PM is decided such that the volume of the piston bowl remains constant and the height of the computational domain is not affected. As a result, the porosity of the PM is found to be 67%. In case of PM combustion, silicon carbide (SiC) is considered as the material for the analysis. The three-dimensional (3D) modeling and meshing of the combustion chambers are performed in ANSYS 17.1-FLUENT software. The baseline specification of the engine, on the basis of which the parameters are set, is of Kirloskar TV1 model with bore and stroke length of 87.5 mm and 110 mm, respectively.

The compression ratio is maintained at 7 for both the domains (without and with PM). The simulation is carried out for the crank angle range of  $50^\circ$  BTDC to  $50^\circ$  ATDC, as during this range the primary combustion behavior is observed. Hence, the maximum height of the computational domain is 42.74 mm. This is the height of the computational domain at the start of simulation and will be attained again once the simulation is completed in the expansion stroke.

### 3.2 Meshing

The present work is carried out with time-dependent variation with dynamic mesh motion. Therefore, the meshing elements are of hexahedral and tetrahedral types for better convergence and accuracy. To maintain the quality of dynamic mesh, skewness factor of 0.84 is found to be optimum for both hemispherical and cylindrical piston bowl computational domain. The meshing of the cylindrical part is performed with hexahedral elements, since it participates in both the compression and the expansion processes. The piston bowl is meshed with tetrahedral elements. This is because with minimum node points the simulation can be performed and significant computational time can be saved. The cylindrical PM zone is, however, meshed with hexahedral elements. The computational domains with aforesaid meshing are represented in Fig. 3.

### 3.3 Grid Independence Test

The grid independence test is essential to determine the optimum mesh, where a fairly accurate solution for a



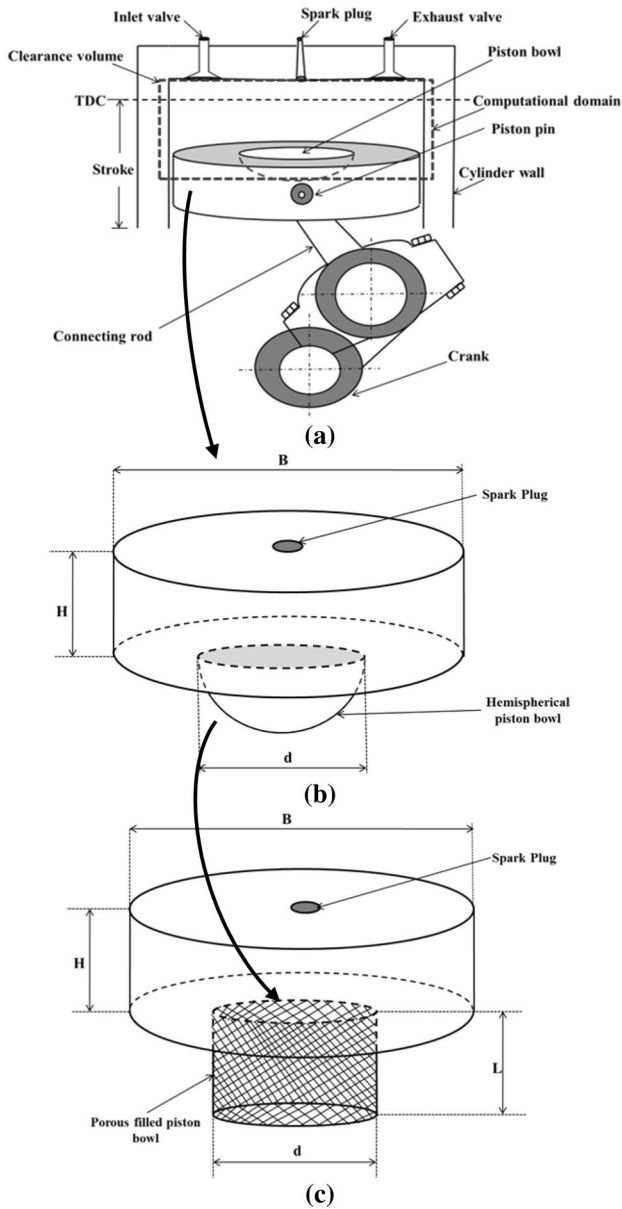


Fig. 2 Schematic diagrams of a piston cylinder arrangement, b computational domain without PM, c computational domain with PM

problem can be found at the expense of least computational resources. The test was performed for the computational domain without PM at full-load condition. The variations of the mean total pressure with respect to the variation of grids are shown in Table 2, and the grid variations on mean total pressure at different crank angles are shown in Fig. 4.

The solutions for element sizes of 1.1 mm and 1.2 mm are within considerable range. Hence, 1.1 mm as element size is considered for the further computational analysis.

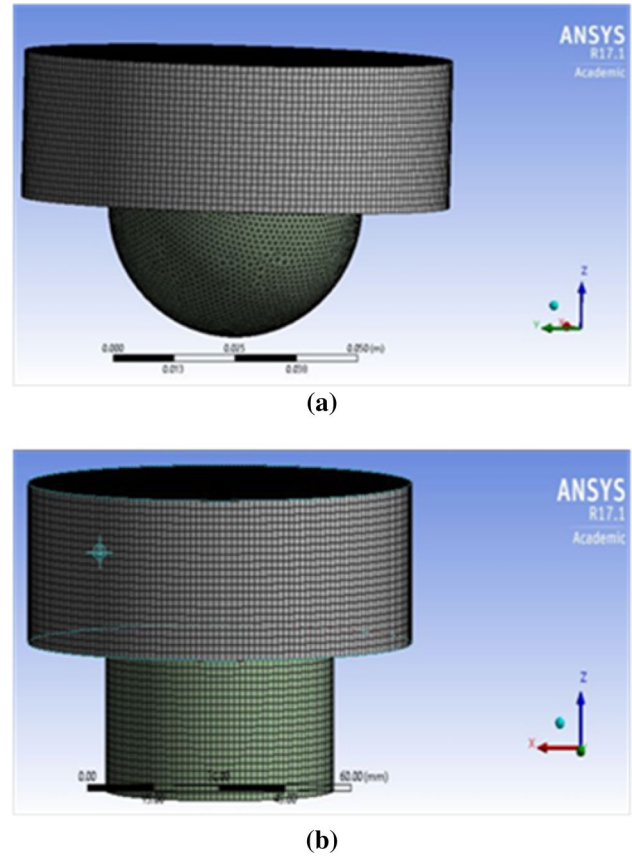


Fig. 3 Meshing of computational domain a without PM, b with PM

Table 2 Peak pressure variation at different element sizes

Element size (mm)	Nodes	Elements	Peak pressure (Pa)
1.3	205,394	335,010	1,998,806.10
1.2	268,389	434,809	1,992,497.67
1.1	409,687	681,249	1,992,314.50

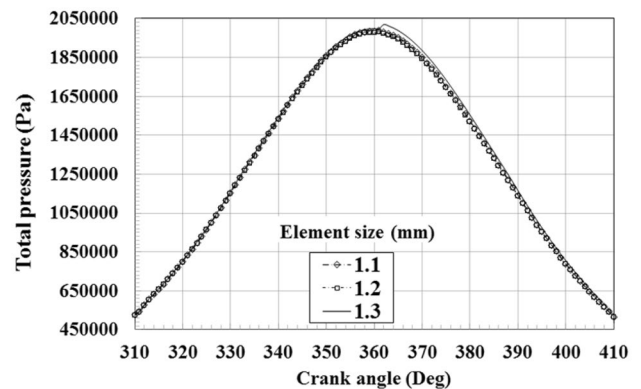


Fig. 4 Grid independence test

### 3.4 Computational Approach

The combustion behavior inside the IC engine is a highly complex phenomenon. During the propagation of flame front, the combustion of unburnt reactants occurs, which converts unburnt premixed reactants to burnt products. The premixed combustion model, especially for SI engine, considers the reacting flow field to be divided into regions of burnt and unburnt species, separated by the flame sheet. The flame front propagation is modeled by solving a transport equation for the density-weighted mean reaction progress variable as given in Eq. 1 (Heywood 1988):

$$\frac{\partial \bar{\rho} \bar{c}}{\partial t} + \frac{\partial \bar{\rho} \tilde{u}_j \bar{c}}{\partial x_j} = \frac{\partial}{\partial x_j} \left( \frac{\mu_T}{S_{c_T}} \frac{\partial \bar{c}}{\partial x_j} \right) + \rho S_c \quad (1)$$

where,  $\bar{c}$ ,  $S_{c_T}$ ,  $S_c$  are the reaction progress variable, turbulent Schmidt number and reaction rate source term, respectively. The progress variable is defined as a normalized sum of the product species as given in Eq. 2:

$$\bar{c} = \frac{\sum_{k=1}^n Y_k}{\sum_{k=1}^n Y_{k,eq}} \quad (2)$$

The simulation is carried out with premixed combustion model. The  $\text{NO}_x$  model is also applied to calculate its different compositions, namely NO, HCN,  $\text{NH}_3$  and  $\text{N}_2\text{O}$  (Park and Kaviany 2002).

### 3.5 Governing Equations

The computational methodology in ANSYS 17.1-FLUENT utilizes the partial differential equations of flow variables to calculate and simulate numerous kinds of analyses concerning the fluid flow. The essential governing equations utilized are mass, momentum and energy conservation equations. The continuity equation or the mass conservation equation for a fluid flow through PM is expressed (Eq. 3) as (Stone 1997):

$$\phi \frac{\partial}{\partial t} + \frac{\partial}{\partial x_j} (\rho u_j) = \dot{m} \quad (3)$$

where,  $\rho$  is the fluid density,  $u_j$  is the  $j$ th Cartesian component of instantaneous velocity, and  $\phi$  is the porosity of the medium. This equation is valid for the incompressible as well as compressible flow. Moreover,  $\dot{m}$ , the rate generated in the system, can be defined as the mass added to continuous phase from the dispersed second phase such as the vaporization of the liquid droplets or any other user-defined sources.

The conservation of momentum in  $i$ th direction for an inertial reference frame can be explained (Eq. 4) as (Stone 1997):

$$\frac{\partial}{\partial t} (\rho u_i) + \frac{\partial}{\partial x_j} (\rho u_i u_j) = \frac{\partial p}{\partial x_i} + \frac{\partial \tau_{ij}}{\partial x_j} + \rho g_i + F_i \quad (4)$$

where,  $p$  is the static pressure,  $\tau_{ij}$  is the stress or tensor,  $\rho g_i$  is the gravitational body force, and  $F_i$  is the external body force from interaction with dispersed phase in  $i$ th direction. The stress tensor in Eq. 5 is given as below:

$$\tau_{ij} = \mu \left( \frac{\partial u_i}{\partial x_j} + \frac{\partial u_j}{\partial x_i} \right) - \frac{2}{3} \mu \left( \frac{\partial u_k}{\partial x_k} \right) \delta_{ij} \quad (5)$$

where,  $\mu$  is the fluid dynamic viscosity and  $\delta_{ij}$  is the Kronecker delta.

The energy conservation equation can be written (Eq. 6) as (Stone 1997):

$$\frac{\partial}{\partial t} (\rho e) + \frac{\partial}{\partial x_i} [u_i (\rho e + p)] = \frac{\partial}{\partial x_i} \left[ K_{\text{eff}} \frac{\partial T}{\partial x_i} - \sum_j h_j J_j + u_j (\tau_{ij})_{\text{eff}} \right] + S_h \quad (6)$$

where,  $K_{\text{eff}}$  is the effective conductivity, i.e.,  $k + k_t$  (where,  $k_t$  = turbulent thermal conductivity),  $J_j$  is the diffusion flux of species  $j$ ,  $S_h$  is the additional volumetric heat source (example: heat of chemical reaction),  $h$  is the sensible enthalpy, and  $e$  is the specific total energy.

### 3.6 Viscous and Inertial Resistance

The PM model of ANSYS 17.1-FLUENT requires the input values of viscous resistance ( $1/\alpha$ ) and inertial resistance ( $\beta$ ). These constants are used to determine the effect of porosity in PM combustion. The viscous resistance is obtained from Darcy's law given by Eq. 7 (Nield and Bejan 2006):

$$\alpha = \frac{D_p}{160} \times \frac{\phi^3}{(1 - \phi^2)} \times S^2 \quad (7)$$

where  $D_p$ ,  $\phi$  and  $S$  are mean pore diameter, porosity and Sphericity, respectively.

The inertial resistance is obtained from Forchheimer's equation expressed in Eq. 9 (Bejan 2004):

$$-\frac{dP}{dx} = \frac{\mu}{K} u + \beta \rho u^2 \quad (8)$$

where,

$$\beta = \frac{3.5}{D_p} \times \frac{(1 - \phi^2)}{\phi^3} \times \frac{1}{S} \quad (9)$$

where,  $-dP/dx$  is the externally controlled pressure gradient,  $\mu$  is the dynamic viscosity,  $u$  is the component of velocity

along the direction of flow, and  $K$  is an empirical constant called permeability.

### 3.7 Effective Conductivity in the PM

The effective thermal conductivity of PM includes the fluid and solid conductivities as shown in Eq. 10 (Bejan 2004):

$$k_{\text{eff}} = \phi k_f + (1 - \phi) k_s \quad (10)$$

where,  $\phi$  is for porosity of PM,  $k_f$  is the fluid thermal conductivity, and  $k_s$  is the solid thermal conductivity.

### 3.8 Peclet Number

Flame quenching processes are analyzed by relating the heat release within the flame to the heat loss to the walls under conditions, where just quenching occurs. The parameter, which identifies flame quenching is called Peclet number ( $Pe$ ) (Ergun 1952). It is a global parameter, which is approximately constant for any given geometrical configuration. It is the product of Reynolds number ( $Re$ ) and Prandtl number ( $Pr$ ). There are number of ways of identifying  $Re$  for use in comparing flow characteristics and heat transfer in engines of different sizes, speeds and geometries. Choosing the best characteristics length and velocity is sometimes difficult. One way of defining  $Re$  for engines that fairly correlates data is given by Eq. 11 as (Bejan 2004):

$$Re = \frac{ul^{1/2}}{\nu} \quad (11)$$

where,  $l^{1/2}$  is the characteristics length of the effective pore diameter, and  $\nu$  is the kinematic viscosity of gas in the cylinder. Similarly, Prandtl number ( $Pr$ ) can be represented by (Eq. 12) as:

$$Pr = \frac{\mu_g \times c_p}{k_f \times \phi + (1 - \phi) \times k_s} \quad (12)$$

where,  $c_p$  is the specific heat of the mixture at constant pressure. The  $Pe$  is a significant term for flame propagation in PM. The value of critical  $Pe$  is 65. Below this value, the flame is reported to be quenched. Moreover, it should be within the permissible limit of  $65 \pm 45$  (Trimis and Wawrzinek 2004).

### 3.9 Heat Release Rate

Heat release rate (HRR) is the rate, at which the chemical energy of the fuel is released in the combustion chamber per degree of crank angle. Heat release rate for a combustion process can be calculated from the in-cylinder pressure values using the first law of thermodynamics as expressed in Eq. 13 (Ceper et al. 2016):

$$\frac{dQ}{d\theta} = \frac{\gamma}{\gamma - 1} P \frac{dV}{d\theta} + \frac{1}{\gamma - 1} V \frac{dP}{d\theta} \quad (13)$$

where,  $Q$  is the heat release in a process,  $\gamma$  is the specific heat capacity ratio,  $\theta$  is the crank angle,  $P$  is the in-cylinder total pressure, and  $V$  is the cylinder volume at particular crank angle. The above equation is used to calculate the heat release rate at all the load conditions.

### 3.10 Laminar Flame Velocity

The velocity of laminar flame,  $S_L$ , is defined by Eq. 14 as mentioned below (Heywood 1988):

$$S_L = S_{L,o} \left( \frac{T_u}{T_o} \right)^\alpha \left( \frac{P}{P_o} \right)^\beta \quad (14)$$

where,  $T_o = 298$  K and  $P_o = 1$  atm are the reference temperature and pressure and  $S_{L,o}$ ,  $\alpha$  and  $\beta$  are constant for a given fuel, equivalence ratio and burned gas diluents fraction.

### 3.11 Input Parameters for the Computational Analysis

The computational analysis is performed in ANSYS 17.1-FLUENT. The computational domain is initialized based on the experimental values of the pressure and temperature at  $50^\circ$  BTDC. In the present work, part simulation is carried out for the crank angle range of  $50^\circ$  BTDC to  $50^\circ$  ATDC, which do not include the processes of the intake ports. The reason of using  $50^\circ$  BTDC to start the simulation is that the standard spark timing of the equivalent baseline engine is  $48^\circ$  BTDC. Further, the simulation is continued up to  $50^\circ$  ATDC, owing to have the same height of expansion of computational domain, as it was available, when simulation was started at  $50^\circ$  BTDC. Moreover, the intake and exhaust valves remain closed during the simulated crank angles. Hence, to make the work computationally viable with the available computational facility at NIT Meghalaya, complete simulation is avoided. The following parameters are taken as input to ANSYS 17.1-FLUENT (Tables 3, 4). The  $k-\epsilon$  turbulence model and premixed combustion model are considered in the study. The spark ignition model has also been activated. The location and heat flux for the spark plug are being specified.

### 3.12 Boundary Conditions

The mechanism of fluid behavior depends on the initial and boundary conditions taken to discretize the governing equations. The entire computational domain is initialized at  $50^\circ$  BTDC with average value of total pressure ( $P_{\text{total}}$ ) at the



**Table 3** Properties of gasoline

Property	Value
Density (kg/m <sup>3</sup> )	703
Specific heat, $c_p$ (J/kg K)	Piecewise polynomial
Thermal conductivity (W/m K)	Piecewise polynomial
Dynamic viscosity (Ns/m <sup>2</sup> )	Piecewise polynomial
Molecular weight (kg/K mol)	114.228
Laminar flame speed (m/s) <sup>a</sup>	0.398
Heat of combustion (J/kg) <sup>a</sup>	538,299.4
Adiabatic unburnt temperature, $T_u$ (K) <sup>a</sup>	410.48

<sup>a</sup>Calculated parameters for the empirical equations

**Table 4** In-cylinder engine properties

Property	Value
Crank shaft speed (rpm)	1500
Starting crank angle (°)	310
Crank period (°)	410
Crank angle step size (°)	0.5
Crank radius (mm) (Fluent 6.3 Documentation 2010)	55
Connecting rod length (mm) (Fluent 6.3 Documentation 2010)	234

respective load conditions. The boundary values of pressure and temperature at respective load conditions are shown in Table 5.

The dynamic mesh zones are created for the entire domain as listed in Table 6. The dynamic meshing in ANSYS 17.1-FLUENT utilizes three different dynamic meshing schemes, namely, smoothing, layering and remeshing. For the present problem layering method is

enabled. The combustion zone, porous zone and moving piston bowl are assigned with the rigid body condition, while the head is assigned with stationary wall condition. In addition, the events occurred at the specific crank angles are being specified. The inputs for defining PM zone in the computational domain are shown in Table 7.

The solution method for pressure–velocity coupling is considered with the pressure-implicit scheme with splitting of operators (PISO) scheme. This is because PISO significantly reduces the convergence difficulties associated with the highly distorted meshes.

## 4 Results and Discussion

This experimental work is based on a single-cylinder four-stroke spark ignition engine and performed on the research setup without PM to obtain the baseline data. Comparison of both the results of experimental and CFD simulations are made at no-load, 25%, 50%, 75% and 100% load conditions. Moreover, the mass fractions of the fuel burned are also calculated for all the load conditions. As the standard spark timing of the engine, the specification of which is considered for the computational modeling, is 48° BTDC. Hence the analysis of the combustion phenomenon is performed for the crank angle duration, starting from 50° BTDC to 50° ATDC. The CFD analysis of domains (without and with PM) is done on the basis of in-cylinder average values of total pressure, total temperature and turbulent kinetic energy of the domain. In addition, emission analysis is also performed on the basis of the production of NO<sub>x</sub> for both the domains.

**Table 5** Boundary conditions at different load conditions

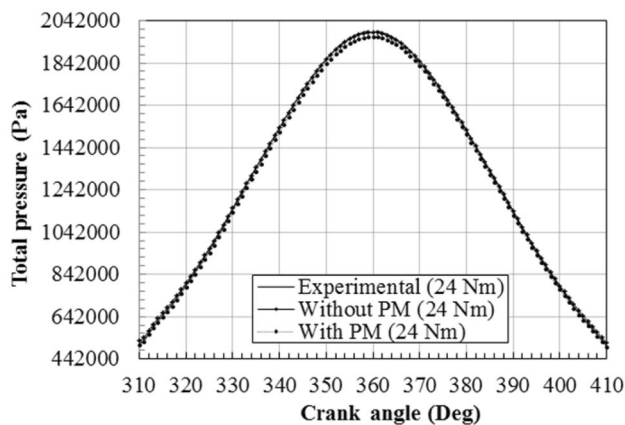
Zones	Boundary type	Load condition	Total pressure (Pa)	Temperature (K)	$\Phi$
Top wall	Wall	No load	244,000	410.48	0.68
		25%	291,000	430.32	0.71
		50%	363,000	440.34	0.78
		75%	376,000	450.05	0.83
		100%	506,000	496.46	0.93
Combustion zone	Wall	No load	244,000	410.48	0.68
		25%	291,000	430.32	0.71
		50%	363,000	440.34	0.78
		75%	376,000	450.05	0.83
		100%	506,000	496.46	0.93
Piston surface	Wall	No load	244,000	410.48	0.68
		25%	291,000	430.32	0.71
		50%	363,000	440.34	0.78
		75%	376,000	450.05	0.83
		100%	506,000	496.46	0.93

**Table 6** Conditions for dynamic meshing

Zone	Body	Motion	Lift/stroke (mm)	Cell height (mm)
Domain	Rigid	(0, 0, 1)	23.47	–
Head	Stationary	–	–	1
Piston surface	Rigid	(0, 0, 1)	23.47	–
Piston porous domain	Rigid	(0, 0, 1)	23.47	0

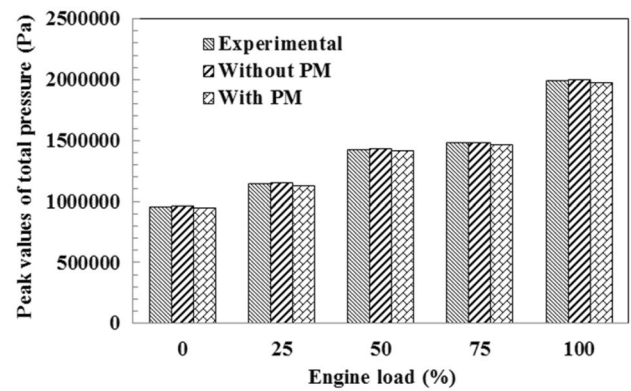
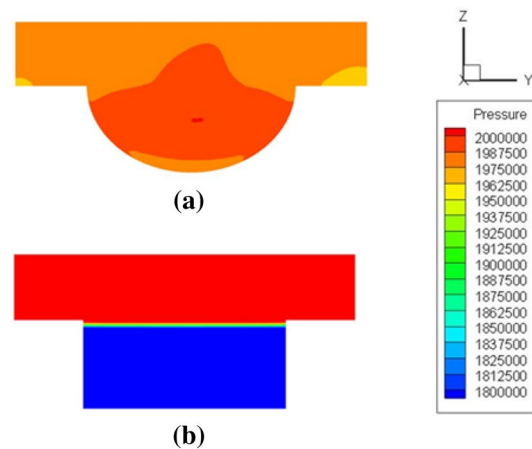
**Table 7** Properties of PM

Property	Value
Mean pore diameter, $D_p$ (mm)	1.6
Porosity, $\phi$	0.67
Sphericity, $S$	0.8
Viscous resistance in PM ( $1/m^2$ )	33,149,332.78
Inertial resistance ( $1/m$ )	3000

**Fig. 5** Variation of total pressure with crank angle for 100% load condition

#### 4.1 Pressure Variation

Pressure is a very important parameter in studying the behavior of fluid. The variation of in-cylinder pressure with crank angle displacement (CA) is depicted in Fig. 5 for both the experimental (without PM) and computational (without and with PM) domains. The curves are plotted only for full-load condition. The plot shows that the in-cylinder total pressure with PM is lower than without PM. The peak pressure without PM is found to be 963,089.07 Pa and with PM is 943,088.27 Pa, respectively, at 370° CA at no-load condition. The comparison of peak values of total pressure at no load, 25%, 50%, 75% and 100% load

**Fig. 6** Comparison of peak pressure at part load conditions**Fig. 7** Contours of pressure variation at 100% load for **a** without PM, **b** with PM at 361° CA

is depicted in Fig. 6 for the experimental (without PM) and computational (without and with PM) domains. The peak value of total in-cylinder pressure for the computational domain without PM is 1,427,735.52 Pa, whereas with PM it is found to be 1,407,736.12 Pa at 364° CA and for experiment it is 1,422,212.50 Pa, respectively, at 365° CA for 50% load condition. The peak value of total in-cylinder pressure for the computational domain without PM is 1,992,314.50 Pa, with PM is found to be 1,966,568.49 Pa at 361° CA and for experiment is 1,986,868.994 Pa, respectively, at 361° CA for 100% load condition. The contours of pressure variation without and with PM at 100% load condition are shown in Fig. 7.

Lower in-cylinder pressure with PM combustion is reported. As the fluid particles accelerate through the pores, the mass flow rate of the charge increases, which results in a pressure drop throughout the domain. This

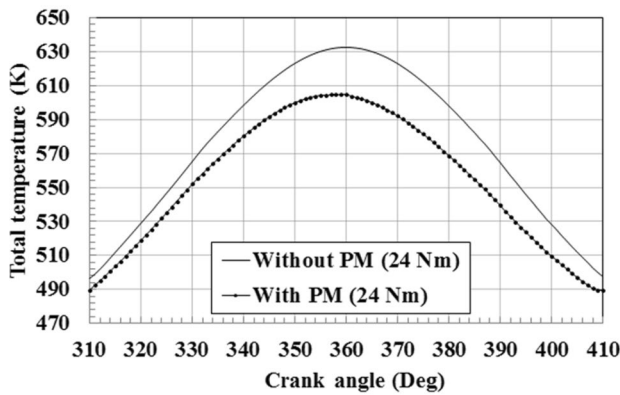


**Fig. 8** Variation of mean total temperature with crank angle for 100% load condition

phenomenon results in high heat transfer rate and homogeneous combustion throughout the domain.<sup>1</sup> Initially, the velocity is very low inside the PM, but when the piston reaches TDC, the velocity of the fuel mixture increases. As a result, the inertial resistance effect contributes the controlled pressure rise in PM cylindrical piston bowl. The percentage of difference between the computational and experimental results without PM was calculated to be 1.1%, 0.35%, 0.38% and 0.27%, respectively, at no load, 25%, 50%, 75% and 100% loads, respectively, at peak pressure condition.

Moreover, the percentage reductions in the peak values of total pressures without PM as compared to with PM for the computational domains are found to be 2%, 1.7%, 1.4%, 1.3% and 1.1%, respectively, at no load, 25%, 50%, 75% and 100% loads, respectively.

## 4.2 Temperature Variation

The variations of the total temperature in the hemispherical piston bowl and porous cylindrical piston bowl for full-load condition at different crank angles are shown in Fig. 8. The plot shows that the in-cylinder total temperature with PM is lower than without PM. The comparison of mean total temperature at all load conditions is shown in Fig. 9. The contours of temperature variations without and with PM at TDC are presented in Fig. 10.

It is found that with the increase in load, the total in-cylinder temperature increases. The maximum average values of total temperatures of domains at 360° CA for without PM

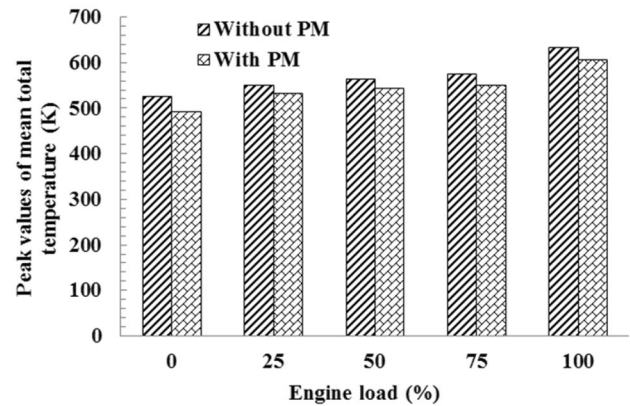


**Fig. 9** Comparison of peak values of mean total temperature at different load conditions at 360° CA

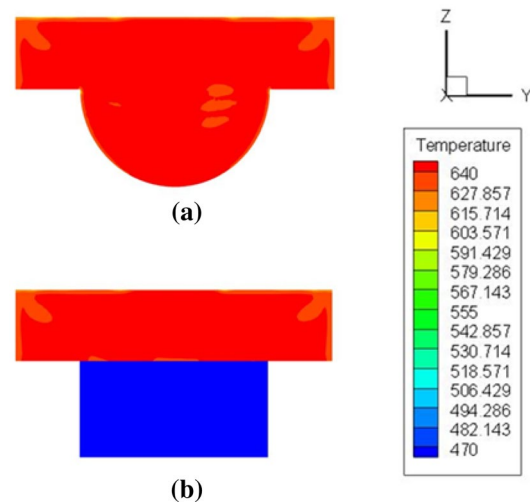


**Fig. 10** Contours of temperature variation at 100% load for **a** without PM, **b** with PM at 360° CA

are found to be 523.96 K, 549.29 K, 562.23 K, 574.29 K and 604.81 K and with PM these are 491.42 K, 530.14 K, 543.29 K, 549.25 K and 632.63 K at no-load, 25%, 50%, 75% and 100% load conditions, respectively. The percentage reduction in temperature are found to be 6.2%, 3.4%, 3.36%, 4.36% and 4.39%, respectively, at no load, 25%, 50%, 75% and 100% loads, respectively, for maximum average value of total temperature of domain. The above result shows the similar trends, as obtained by Mujeebu et al. (2010) in their work on 3D numerical model for the regenerative engine using modified version of the KIVA-3V code. Hence, it confirms a significant reduction in domain temperatures toward the application of PM.

<sup>1</sup> Instruction Manual, Computer Based Four Stroke Single Cylinder Variable Compression Ratio Multifuel Engine with Eddy Current Dynamometer, Tech-Ed Equipment Company, Bengaluru, 560072, Karnataka, India

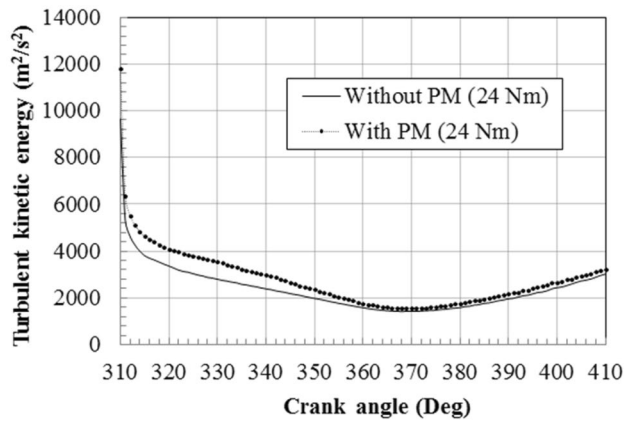


Fig. 11 Variation of TKE with crank angle for 100% load condition

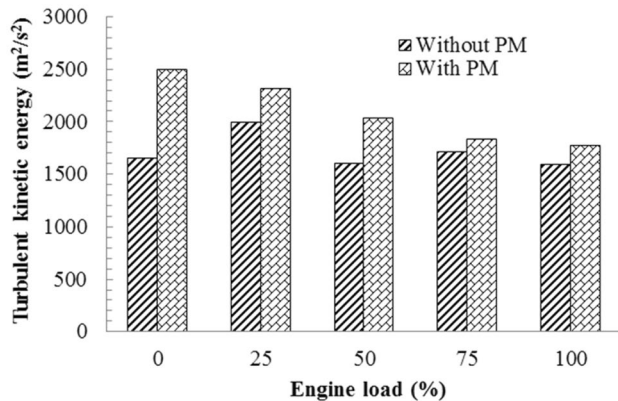


Fig. 12 Comparison of TKE at part load conditions at 360° CA

### 4.3 Turbulent Kinetic Energy Variation

The turbulence consists of randomly dispersed vortices of varying sizes superimposed in the charge flow stream. It is a 3D unsteady random motion, observed in fluids at moderate to high Reynolds number. The turbulence is characterized in terms of turbulent intensity and turbulent kinetic energy. The variations of the turbulent kinetic energy (TKE) in the hemispherical piston bowl and modified porous cylindrical piston bowl at different crank angles are shown in Fig. 11 for 100% load condition. The values of TKE decrease, but the turbulence dissipation rate increases at the end of compression stroke. The comparison of TKE at all the load conditions is performed at 360° CA in Fig. 12. It is found that with the increase in load, the TKE decreases. It is owing to a significant difference between the in-cylinder tumble and swirl components. The swirl continuously weakens by compression, thereby resulting in a decrease in TKE level (Fukang et al. 2015). The physical reason behind the TKE increase with porous media (PM) is due to increased vortices

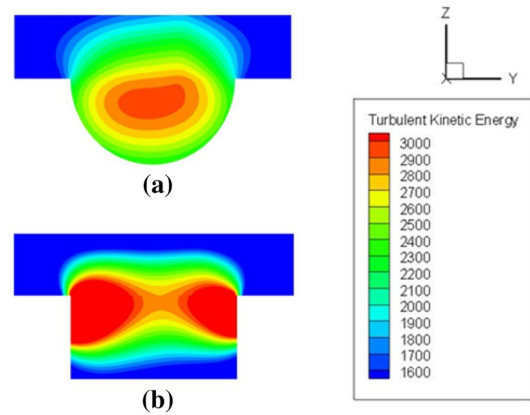


Fig. 13 Contours of TKE variation at 100% load for a without PM, b with PM

within the charge during PM combustion (Singh and Singh 2012). This is discussed by adding two new references as mentioned below. Upon considering the motion of the charge in PM, the fluid is not supposed to move in a streamline motion. The charge moves in the traverses around the pores of the PM (Yuan and Finkelstein 1956). The interaction of the charge at the porous wall increases the friction coefficient due to the increased momentum exchange with the main flow. This phenomenon leads to the increase in the turbulence within the charge flowing through PM. This is appreciated physically by the increase in TKE level. The maximum values of TKEs during computational study at 360° CA for without PM are found to be 1651.19  $\text{m}^2/\text{s}^2$ , 1985.33  $\text{m}^2/\text{s}^2$ , 1596.64  $\text{m}^2/\text{s}^2$ , 1708.96  $\text{m}^2/\text{s}^2$  and 1582.28  $\text{m}^2/\text{s}^2$ , and with PM, the values reported are 2494.62  $\text{m}^2/\text{s}^2$ , 2314.23  $\text{m}^2/\text{s}^2$ , 2033.24  $\text{m}^2/\text{s}^2$ , 1827.96  $\text{m}^2/\text{s}^2$  and 1771.13  $\text{m}^2/\text{s}^2$  at 0%, 25%, 50%, 75% and 100% load conditions, respectively. The turbulent kinetic energy does not remain constant during compression and power stroke. The formation of eddies is due to the resistance experienced by the fluid flowing inside the PM. These eddies enhance the heat transfer rate of the charge. This results in homogeneous combustion of the charge inside the combustion zone.

The percentage enhancements in the TKEs due to application of PM are found to be 33.83%, 14.21%, 21.47%, 6.5% and 10.66% at no load, 25%, 50%, 75% and 100% loads, respectively. It is found that the maximum enhancement of TKE is at no-load condition. The contours of TKE distribution for the domains without and with PM are shown in Fig. 13.

### 4.4 NO<sub>x</sub> Emissions

The variations of the NO<sub>x</sub> emissions without and with PM at different crank angles are shown in Fig. 14. NO<sub>x</sub> emission increases with the increase in load conditions. Due to the increase in temperature, there is an increase in NO<sub>x</sub>



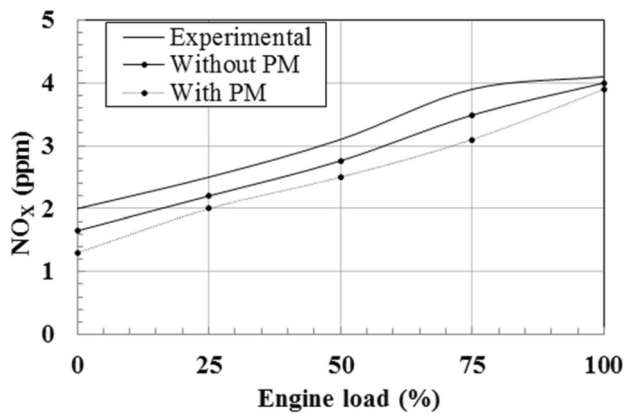


Fig. 14 NO<sub>x</sub> emissions at different engine load conditions

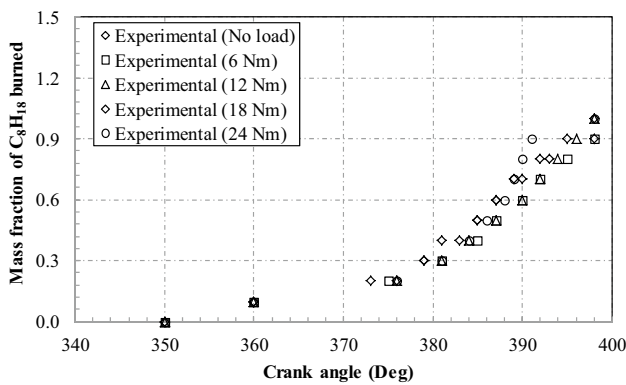


Fig. 15 Experimental results of the variation of mass fraction of C<sub>8</sub>H<sub>18</sub> burned

emissions at higher loads. At higher loads the combustion is more effective and also a lesser amount of residual gases remain inside the combustion chamber. As mentioned in the different literature, formation of NO<sub>x</sub> is a strong function of combustion temperature (Suhās et al. 2013).

The percentage differences of NO<sub>x</sub> emissions in experimental and computational domains without PM is found to be 17.5%, 12%, 10.96%, 10.5% and 2.4% for no load, 25%, 50%, 75% and 100% loads, respectively. The significant difference in experimental and computational results is primarily because of the impurities present in the fuel (e.g., lead, fuel impurities). Moreover, it is observed that NO<sub>x</sub> formation is significantly reduced with PM. The percentage reductions in NO<sub>x</sub> emissions at no load, 25%, 50%, 75% and 100% are found to be 21%, 9%, 9.4%, 11.1% and 2.5%, respectively. This is because of the fact that the residual time of the fuel burning is enhanced in the presence of PM, which results in better mixing and evaporation of the charge. Moreover, PM is also heated up by the flame, which results in flame stabilization at high temperature. This process may reduce the fuel consumption.

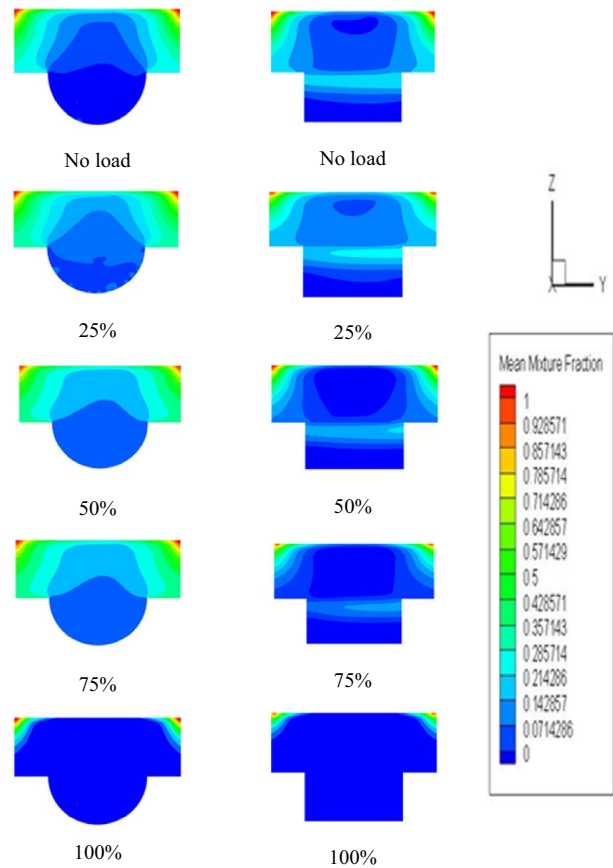


Fig. 16 Computational results of the variation of mean mass fraction of C<sub>8</sub>H<sub>18</sub> for a without PM, b with PM at 396° CA

### 4.5 Mass Fraction Burned

The variation of mass fraction of C<sub>8</sub>H<sub>18</sub> at no-load, 25%, 50%, 75% and 100% load conditions is shown in Fig. 15. The rate of burning is proportional to increase in the concentrations of fuel supplied.

It implies that with the increase in engine loads, the burning rate is also increased. The variation in the mass fraction of C<sub>8</sub>H<sub>18</sub> is studied after the spark ignition at 312° CA. It is seen that the burning of the charge starts from 350° and it is completely burned at 398° crank angle under all the loading conditions. The burning rate is highest for the full-load condition followed by 75%, 50%, 25% and no load, respectively. The contours of mean mixture fractions without and with PM at 396° crank angle are shown in Fig. 16 for all the load conditions. This can be seen that maximum mass fraction of C<sub>8</sub>H<sub>18</sub> is burnt at full-load condition followed by 75%, 50%, 25% and no loads, respectively.



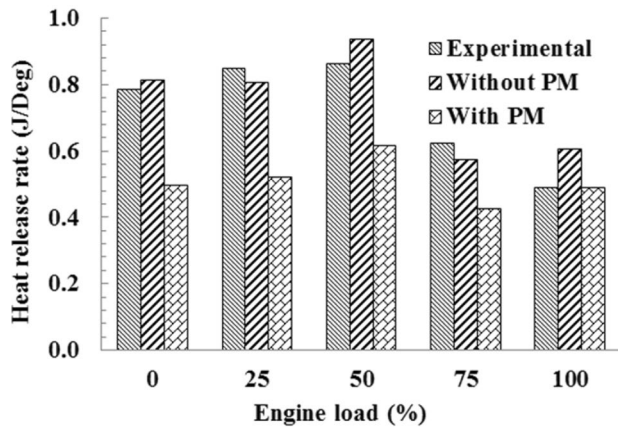


Fig. 17 Variations of heat release rate at different engine load conditions at 360° CA

#### 4.6 Heat Release Rate

Heat release rate (HRR) is the rate at which the chemical energy of the fuel is released in the combustion process. When the engine load increases, the combustion heat release takes place in a shorter time due to a faster combustion speed, which results in a higher cylinder pressure (Ceper et al. 2016). Heat release rate,  $\frac{dQ}{d\theta}$ , is calculated from Eq. (13). The different values of pressure and volume at each crank angle obtained from both computational (without and with PM) and experimental (without PM) domains are then utilized to calculate the heat release rates at different load conditions. The HRR values are found to be 0.811 J/°, 0.805 J/°, 0.936 J/°, 0.571 J/° and 0.603 J/° at no-load, 25%, 50%, 75% and 100% load conditions, respectively. The values of HRR with PM are 0.493 J/°, 0.519 J/°, 0.613 J/°, 0.426 J/° and 0.489 J/°. The HRR values for the experiment are found to be 0.785 J/°, 0.847 J/°, 0.861 J/°, 0.623 J/° and 0.488 J/° at no-load, 25%, 50%, 75% and 100% load conditions, respectively, at TDC condition. It is also found that HRR for the computational domain with PM is lower than without PM. A comparison is made between instantaneous rates of heat release at TDC positions at all the load conditions as shown in Fig. 17.

The percentage difference in the experimental and computational results without PM is calculated as 3.2%, 4.9%, 8%, 8.3% and 19.07%, respectively, at no load, 25%, 50%, 75% and 100% loads, respectively. At 370° CA, the difference in the HRR values are found to be 2.6%, 12.7%, 23%, 41% and 66.41%, respectively, for all the loads studied. The variations of HRRs for experimental, computational domains (without and with PM) at full-load condition are shown in Fig. 18. It can be observed (Table 8) that the HRRs are higher after TDC, under all load conditions. It is due to high heat capacity of the SiC, which absorbs the heat of combustion during compression stroke and releases that heat in the expansion

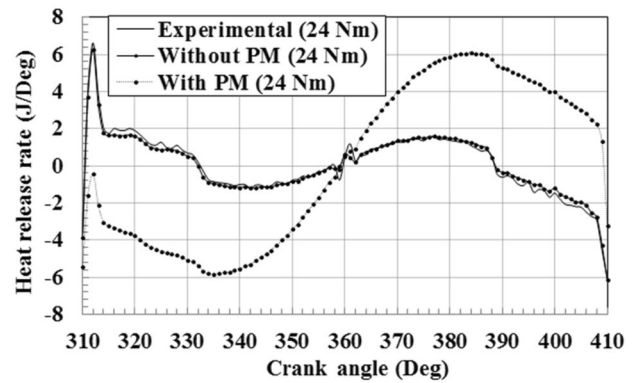


Fig. 18 Variation of heat release rate with crank angle for 100% load condition

stroke. This results in the enhancement in the combustion process and lesser production of unburnt hydrocarbons. It is also observed that difference in HRR, without and with PM, increases with the increase in the loads.

#### 4.7 Peclet Number

The average velocity through the pores is found to be 10.367 m/s from the simulation results with PM at full-load condition. Using this value,  $Re$  and  $Pr$  are calculated from Eqs. (11, 12). The product of  $Re$  and  $Pr$  provides  $Pe$ , which was found to be 83.7. This is outside the range of flame quenching.

### 5 Conclusions

Some of the concluding remarks of the present works are as follows:

- The peak pressure (1,966,568.49 Pa) and temperature (632.63 K) with PM at 24 Nm are found to be lower than without PM.
- The maximum value of TKE at TDC without PM is found to be 1582.28 m<sup>2</sup>/s<sup>2</sup>, whereas with PM it is 1771.13 m<sup>2</sup>/s<sup>2</sup> at 100% load condition, respectively.
- The concentration of NO<sub>x</sub> emission is significantly reduced by the use of PM for all the load conditions. The percentage reductions in NO<sub>x</sub> emissions at no load, 25%, 50%, 75% and 100% loads are found to be 21%, 9%, 9.4%, 11.1% and 2.5%, respectively.
- The burning rate is highest at the full-load condition followed by 75%, 50%, 25% and no load, respectively.
- At 370° CA, the differences in the HRR values between non-porous and porous domains are found to be 2.6%, 12.7%, 23%, 41% and 66.41%, respectively, which implies PM combustion is more effective at high-load conditions.

**Table 8** Comparison of peak HRR at respective CA for experimental, computational (without and with) PM

Sl no.	Load (%)	Peak HRR (E) (J/°)		Peak HRR without PM (C) (J/°)		Peak HRR with PM (C) (J/°)	
		CAD	Value	CAD	Value	CAD	Value
1	0	374	1.40	373	1.44	384	2.83
2	25	371	2.41	371	2.20	373	3.32
3	50	367	2.66	369	2.53	371	3.54
4	75	364	3.24	364	3.21	368	3.72
5	100	362	3.89	361	3.69	363	4.83

- The average velocity through the pores is found to be 10.367 m/s from the simulation. Using this value, Peclet number is found to be 83.7 at full-load condition, which is outside the range of flame quenching.

**Acknowledgements** The authors wish to extend their sincere thanks to Santosh Kumar, Senior Works Manager of TECH-ED Equipment Company, Bangalore, for his support and required guidance in performing the experimental works. Further, sincere gratitude also goes to Nur Alom, Trainee Teacher of Mechanical Engineering, for his assistance in learning ANSYS 17.1-FLUENT.

## References

- Bejan A (2004) Convection heat transfer, 3rd edn. Wiley, New York
- Ceper BA, Yildiz M, Akansu SO, Kahraman N (2016) Performance and emission characteristics of an IC engine under SI, SICAI and CAI combustion modes. *Int J Power Energy* 4:1–8
- Chidambaram K, Thulasi V (2016) Two zone modeling of combustion, performance and emission characteristics of a cylinder head porous medium engine with experimental validation. *Multidiscip Model Mater Struct* 12(3):495–513
- Das S, Kumar S, Debnath BK (2015) CFD analysis of combustion in a Wankel Engine in the presence of Porous Media. In: Poster presentation in the 5th international conference on advances in energy research (ICAER), IIT Bombay, India
- Durst F, Weclas M (2001) A new type of internal combustion engine based on the porous medium combustion technique. *Proc Inst Mech Eng D J Automob Eng* 215:63–81
- Ergun S (1952) Fluid flow through packed columns. *Chem Eng Prog* 48(2):89–94
- Fluent 6.3 Documentation (2010) ANSYS 17.1-FLUENT, Inc. [http://my.fit.edu/itresources/manuals/fluent6.3/help/html/tg/main\\_pre.htm](http://my.fit.edu/itresources/manuals/fluent6.3/help/html/tg/main_pre.htm)
- Fukang M, Changlu Z, Fujun Z, Zhenfeng Z, Shuanlu Z (2015) Effects of scavenging system configuration on in-cylinder air flow organization of an opposed-piston two-stroke engine. *Energies* 8(1):5866–5884
- Hanamura K, Bohda K, Miyairp Y (1997) A study of super-adiabatic combustion engine. *Energy Convers Manag* 38:1259–1266
- Heywood J (1988) Internal combustion engine fundamentals. McGraw-Hill Book Company, New York
- Jamalabadi MYA, Rajabzadeh M, Hooshmand P (2015) Effect of fuel inject angle on the thermal behavior of a 2D axisymmetric non-premixed methane–air flame in vertical cylinder filled by porous media. *Int J Energy Eng* 5(1):1–8
- Jugjai S, Polmart N (2003) Enhancement of evaporation and combustion of liquid fuels through porous media. *Exp Therm Fluid Sci* 27(8):901–909
- Krishna K, Kumar P, Reddy VK, Rao PV, Gugulothu R (2016) A review of porous-media combustion technology applied to IC engine. *Int J Eng Res (IJER)* 5(2):491–494
- Liu H, Xie M, Wu D (2009) Thermodynamic analysis of the heat regenerative cycle in porous medium engine. *Energy Convers Manag* 50(1):297–303
- Mohammadi A, Jazayeri A, Ziabasharhagh M (2012) Numerical simulation of combustion with porous medium in IC engine. *Int J Automob Eng* 2(4):228–241
- Mujeebu M, Abdullah MZ, Mohammad AA, Bakar MZ (2010) Trend in modelling of porous media combustion. *J Prog Energy Combust Sci* 2(1):1–24
- Nield DA, Bejan A (2006) Convection in porous media, 3rd edn. Springer, Berlin
- Park CW, Kaviany M (2002) Evaporating combustion affected by in cylinder reciprocating porous regenerator. *ASME J Heat Transf* 124(2):184–194
- Patel AB, Patel VR, Ambaliya AM (2015) Study of effect of porous media combustion chamber on diesel engine performance and emission: technical review. *Int J Eng Res Technol (IJERT)* 3(2):78–91
- Polasek M, Macek J (2003) Homogenization of combustion in cylinder of CI engine using porous medium. SAE Paper 2003-01-1085
- Shaahangian N, Ghoje J (2010) Investigation of the interaction between diesel spray and porous medium. In: 17th Australian fluid mechanics conference, 5–9th December, Auckland, New Zealand
- Shahangian N, Ghojel J (2010) Investigation of the interaction between diesel spray and porous medium. In: 17th Australian fluid mechanics conference, Auckland
- Shi JR, Xie MZ, Liu H (2011) Two-dimensional numerical study of combustion and heat transfer in porous media combustor-heater. *Proc Combust Inst* 33(2):3309–3316
- Singh B, Singh C (2012) Analysis of vortex motion in porous media. *J Electron Cool Therm Control* 2:32–34
- Stone R (1997) Introduction to internal combustion engines. Society of Automotive Engineers Inc., Warrendale
- Suhas BG, Shivaprasad KV, Kumar GN (2013) Computational and experimental investigation of NO<sub>x</sub> emission of hydrogen blend on a constant speed gasoline engine. *Int J Theor Appl Res Mech Eng* 2(4):121–125
- Trimis D, Wawrzinek K (2004) Flame stabilization of highly diffusive gas mixtures in porous inert media. *J Comput Appl Mech* 5(2):367–381
- Weclas M (2005) Potential of porous-media combustion technology as applied to internal combustion engines. *J Thermodyn* 2010(1):1–39
- Yuan SW, Finkelstein AB (1956) Laminar pipe flow with injection and suction through a porous wall. *Trans Am Soc Mech Eng* 78(4):719–724
- Zhao FQ, Lai MC (1995) The spray characteristics of automotive port fuel injection—a critical review. SAE Technical Paper-950506
- Zhou L, Xie MZ, Luo KH (2014) Numerical study of heat transfer and combustion in IC engine with a porous media piston region. *Appl Therm Energy* 65(1):597–604